Bistable Actuation Based on TiNiHf/Si Shape Memory Nanoactuators

Zixiong Li[1], Gowtham Arivanandhan[1], Sabrina M. Curtis[2, 3], Eckhard Quandt[2] and Manfred Kohl[1, *]
[1] Institute of Microstructure Technology, Karlsruhe Institute of Technology (KIT), 76344 Eggenstein-Leopoldshafen, Germany
[2] Institute for Materials Science, Kiel University (CAU), 24143 Kiel, Germany
[3] Department of Materials Science and Engineering, University of Maryland, College Park, MD 20742, USA
[*] Correspondence: manfred.kohl@kit.edu

Abstract

We present the design and analytical model of a bistable nanoactuator consisting of a PMMA/TiNiHf/Si trimorph layer composite, in which the layer of shape memory alloy TiNiHf shows a martensitic phase transformation with wide hysteresis in the temperature range of 50 - 140 °C, while the PMMA layer undergoes a glass transition at 105 °C. We demonstrate that the thickness of the TiNiHf layer can be adjusted down to a critical thickness of 220 nm using a Si substrate with SiO_2 buffer layer without affecting its phase transformation temperatures, which enables the design of ultra-compact bistable actuator devices. The presented model characterizes the bistable actuation stroke as a function of PMMA layer thickness at room temperature. The obtained optimal layer thicknesses allow for the development of a process flow for nanofabrication of the trilayer composite.

1 Introduction

Nowadays, there is a growing demand on micro- and nano-actuators for next generation Si-based nanomechanical and nanophotonic applications requiring large stroke compared to their size, high power efficiency and compatibility to Si technology [1]. Among the potential actuation mechanisms, shape memory alloy (SMA) actuation is highly attractive as it offers a large work output in the order of 10^7 J/m^3 [2] and favourable downscaling properties. Research on photonic switches based on SMA nanoactuators [1, 3] showed the appealing advantage of actuator footprint in the order of 10 µm² compared to electrostatic actuation mechanisms like comb-drive actuators. For such applications, the SMA thin film is sputtered on the Si device layer [4]. Hence, the design and optimization of nanoactuation performance requires a model for bi- and multilayer SMA/Si composite beams.

In this paper, we investigate a bistable mechanism, which makes use of the large hysteresis of a TiNiHf film sputtered on a flexible substrate and an additional polymethyl methacrylate (PMMA) layer with matched glass transition temperature T_g in between SMA's phase transformation temperatures [5, 6]. As the polymer becomes hard below T_g, it can fix the actual shape of the TiNiHf/substrate composite upon cooling below T_g. Thus, cooling from high temperature austenite state will fix the austenitic shape, while cooling from martensitic state at a temperature above T_g will fix the corresponding martensitic shape. So far, this bistable mechanism has been realized on mm-scale [5, 7]. Here, we explore possible size effects for decreasing film thickness and present a model to describe and optimize the temperature-dependent deflection of bistable PMMA/TiNiHf/Si multilayer actuators.

2 Background

Theoretical models based on classical Eulerian beam theory have been investigated to simplify and speed up the design and optimization of bi- and multilayer beam actuators compared to computationally intensive finite element models. Timoshenko [8] firstly proposed the theoretical solution of deflection of a bilayer beam with different but temperature-independent elastic moduli and coefficients of thermal expansion (CTE) under thermal effect. Moulin et al. [9] firstly used this result to analyse micromechanical bilayer thermal sensors. A similar analysis was made for the design of a SRN/SU-8 bimorph temperature sensor by Larsen et al. [10]. To meet the rapid development of actuators and sensors with cantilever configurations in microelectromechanical systems (MEMS), models considering additional effects were proposed. Hsueh et al.[11] studied thermal induced stress distribution in a three-layer structure sandwiching a graded layer. For more general applications, Zhang [12] extended the bilayer model to a multilayer system. Further work focussed on the influence of gradient residual stress in multilayer structures [13, 14]. Beam models considering large deflection were also investigated, which do not satisfy the assumptions of Eulerian beam theory [15, 16].

In applications of micro- and nano-actuators, Joule-heating is a common method to control thermal actuators, which gives rise to inhomogeneous temperature distributions. Jiang et al. [17] considered this deviation and proposed an electro-thermo-mechanical model to gain more precise prediction of deflection. In addition, size and scaling effects may cause large effects on actuator performance [18]. Therefore, these effects receive much attention in order to ameliorate the classical beam theory. One of the most popular theories is couple stress theory [19-23]. Tan et al. [24] integrated this theory to Jiang's model [17] and obtained a sophisticated model predicting more accurately the deflection of multilayer SiO_2/Ti/Si cantilever beams.

ISBN: 978-3-8007-6203-3

3 Size-dependent phase transformation of TiNiHf films

Size effects play an important role in the downscaling of SMA-based actuators, as they may influence SMA properties such as phase transformation temperatures and thermal hysteresis width. Monitoring the temperature-dependent electrical resistance is a common way to reveal information of phase transformation of SMA films [25, 26]. For this purpose, a four-probe electrical resistance measurement is conducted in a thermostat to control the ambient temperature change under quasi-stationary condition.

Thin TiNiHf films with different thicknesses ranging from 110 nm to 5 µm are prepared using DC magnetron sputtering on 585 µm thick Si and SiO_2/Si substrates with 1000 nm SiO_2 buffer layer. Rapid thermal annealing (RTA) at 635 °C for 5 min follows the sputtering process to crystallize deposited amorphous film, as described in [6]. **Fig. 1** presents a temperature-resistance curve of a 220 nm thick TiNiHf film on a SiO_2/Si substrate. Despite the small film thickness, the transformation is comparable to the phase transformation of bulk TiNiHf. Four phase transformation temperatures, i.e. martensitic start and finish temperatures (M_s and M_f), austenitic start and finish temperatures (A_s and A_f), are determined by the tangential method. The hysteresis width of curve is defined by:

$$\Delta T = \frac{(A_f + A_s - M_s - M_f)}{2} \quad (1)$$

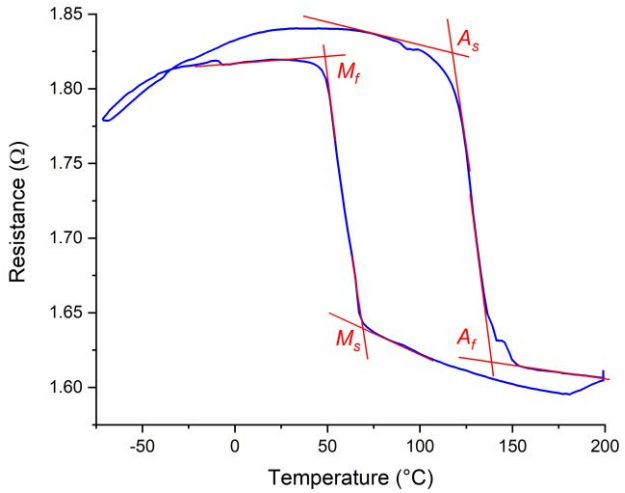

Figure 1: Temperature-electrical resistance curve of a 220 nm thick $Ti_{40.4}Ni_{48}Hf_{11.6}$ film on a 585 µm Si substrate with 1000 nm thick SiO_2 buffer layer. The martensitic and austenitic start and finish temperatures ($M_{s,f}$ and $A_{s,f}$) are determined by the tangential method.

The thickness dependence of phase transformation temperatures of the prepared TiNiHf films is summarized in **Fig. 2** for both types of substrate. Note that M_f and A_s are not indicated for the 110 nm thick film on Si substrate without SiO_2 buffer layer, because the martensitic transformation does not finish in the investigated temperature range. These measurements reveal a significant change in transformation temperatures and hysteresis width, when the thickness of TiNiHf films on Si substrates reduces from 440 to 220 nm. For TiNiHf films on SiO_2/Si substrates, this change occurs in the thickness range between 220 and 110 nm. These results indicate the existence of a critical thickness limit for nano actuation at room temperature, which is also substrate dependent. Above the critical thickness, the phase transformation properties of TiNiHf film do not show a significant thickness dependence.

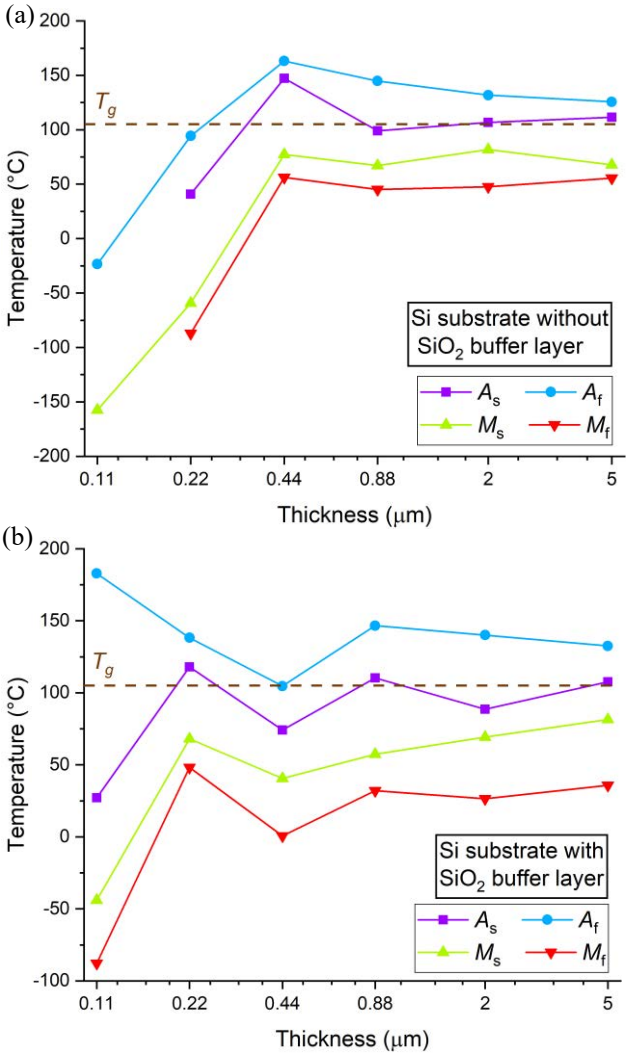

Figure 2: Phase transformation temperatures versus thickness of TiNiHf films on a Si substrate without (a) and with (b) SiO_2 buffer layer. The glass transition temperature of PMMA is also indicated (dashed line).

4 Analytical model of a multilayer beam

4.1 Thermal effect

Considering a general cantilever beam illustrated in **Fig. 3**, the elastic modulus $E(y)$ and beam width $b(y)$ vary along the depth direction (y-axis in **Fig. 3**). Based on the model of Eulerian beam, it can be assumed that beam axis remains

vertical to the cross section of beam after deflection. The stress distribution along the cross section is expressed as:

$$\sigma(y) = E(y)\varepsilon(y) \tag{2}$$

with the strain distribution given by:

$$\varepsilon(y) = \varepsilon_0 + \varphi y - \varepsilon_{inelastic}(y). \tag{3}$$

Here, ε_0 is strain at the centroid z_c of beam cross section, φ is the curvature of bending deformation and $\varepsilon_{inelastic}(y)$ is the strain not contributing to elastic stress, which includes strains such as thermal strain ε_{th}. In case the coefficient of thermal expansion $\alpha(y,T)$ is also a function of temperature, the thermal strain is:

$$\varepsilon_{th}(y) = \int_{T_{ref}}^{T} \alpha(y,T)\,\mathrm{d}T\,, \tag{4}$$

whereby T_{ref} is the reference temperature.

Considering boundary conditions without external loading of quasi-static deformation:

$$N = \int \sigma(y)\cdot b(y)\mathrm{d}y = 0 \tag{5}$$

$$M = \int \sigma(y)\cdot yb(y)\mathrm{d}y = 0 \tag{6}$$

Together with **Eqs.** (1) and (2), ε_0 and φ can be expressed as

$$\varepsilon_0 = \frac{\int \varepsilon_{inelastic}(y)\cdot E(y)b(y)\mathrm{d}y}{\int E(y)b(y)\mathrm{d}y} \tag{7}$$

$$\varphi = \frac{\int \varepsilon_{inelastic}(y)\cdot E(y)(y-z_c)b(y)\mathrm{d}y}{\int (y-z_c)^2 b(y)\mathrm{d}y} \tag{8}$$

In case of small deflection, the deflection value δ is:

$$\delta = -\frac{\varphi}{2}l^2 \tag{9}$$

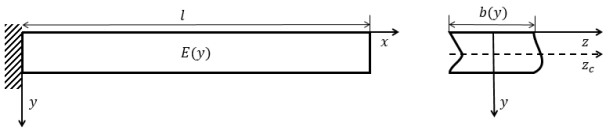

Figure 3: Sketch of a general cantilever beam with varying width and elastic modulus along thickness (y-) direction. Legend: l – beam length, $b(y)$ – width, $E(y)$ – elastic modulus, z_c – distance between centroid of cross section and z-axis.

It is worth noting that in the model above, the temperature T is not a function of spatial position, i.e., temperature inhomogeneity is not considered. However, in conventional parallel beam designs of beam cantilever actuators, the temperature gradient along the beam direction can well reach 50 K/µm [27]. This problem has been mitigated recently by introducing additional folded beams near the fixed end of the beam cantilever [28, 29]. In this case, it is still reasonable to assume homogeneous temperature distribution.

4.2 Shape memory effect

Assuming that the shape memory alloy has different effective elastic moduli at austenitic state E_a and at martensitic state E_m, the average elastic modulus in the phase transformation regime is approximated by the law of mixture:

$$E_{SMA}(T) = E_m\xi(T) + E_a(1-\xi(T)) \tag{10}$$

where $\xi(T)$ is volume fraction of martensitic phase given in the form of logistic function:

$$\xi(T) = \frac{1}{1+\exp[k(T-T')]} \tag{11}$$

The following expressions are used for martensitic transformation:

$$k = \frac{k_0}{M_s - M_f}, \quad T' = \frac{M_s + M_f}{2}$$

and for austenitic transformation:

$$k = \frac{k_0}{A_f - A_s}, \quad T' = \frac{A_s + A_f}{2}$$

with the constant k_0 introduced in [30].

Similarly, the coefficient of thermal expansion is approximated by:

$$\alpha_{SMA}(T) = \alpha_m\xi(T) + \alpha_a(1-\xi(T)) \tag{12}$$

4.3 Model of PMMA

When the temperature decreases below the glass transition temperature T_g, the polymer quickly hardens and its elastic modulus increases from soft E_{hot} to hard E_{cold}. We assume that the elastic modulus $E(T)$ still satisfies a logistic curve during the glass transition:

$$\lg E(T) = \frac{\lg\left(\frac{E_{cold}}{E_{hot}}\right)}{1+\exp\left[k_{PMMA}\left(T-T_g\right)\right]} + \lg E_{hot} \tag{13}$$

whereby k_{PMMA} is a constant depending on the material property. Similarly, the change of thermal expansion coefficient α_{PMMA} is also described by a logistic function during the glass transition. Assuming that this value reduces to zero at infinitely high temperature, it is written as:

$$\alpha_{PMMA}(T) = \frac{\alpha_{cold}}{1+\exp\left(T-T_g\right)} \tag{14}$$

To further describe the viscoelastic properties of PMMA during glass transition, Sun et al. [31] classify PMMA as a kind of shape memory polymers (SMPs) and Xin et al. [32] accordingly propose three consecutive models of SMPs based on (1) theory of viscoelasticity, (2) phase transformation theory, (3) combined theory of the two aforementioned. Here, we adopt the second theory, which introduces a concept of "stored strain" to describe the transition between frozen phase (glassy state below T_g) and active phase (rubbery state above T_g). More information can be found in [32, 33].

5 Analytical results

The material properties of Si, TiNiHf and PMMA are taken from [29, 34]. We stack a three layer composite, i.e. PMMA/TiNiHf/Si from top to bottom, whereby each layer has the same width. **Fig. 4** demonstrates the mechanism of bistable actuation of the three-layer system. Assuming that the whole structure is in a stress-free state at the annealing temperature, thermal stress accumulates during cooling.

ISBN: 978-3-8007-6203-3

By referring to a TiNiHf/Si bilayer beam (red line), the deflection reaches a peak upon cooling and experiences a drop when reaching the martensitic transformation regime. Thereby, the intrinsic stress is released to a large extent due to accommodation of martensite variants. After the phase transformation has finished, the deflection curve increases again. Consequently, there are two deflection states of the bilayer beam before and after phase transformation, which can be stabilized by the third PMMA layer when it becomes hard below T_g. Depending on the heating and cooling path, either one of the two deflection states will be fixed as indicated in **Fig. 4**: (1) Heating from room temperature (RT) to a heated state above A_f and subsequent cooling back to RT (green lines) results in the large deflection state (*State I*). (2) Heating from RT to an intermediate temperature $T_g < T < A_s$ and subsequent cooling back to RT (blue lines) results in the small deflection state (*State II*).

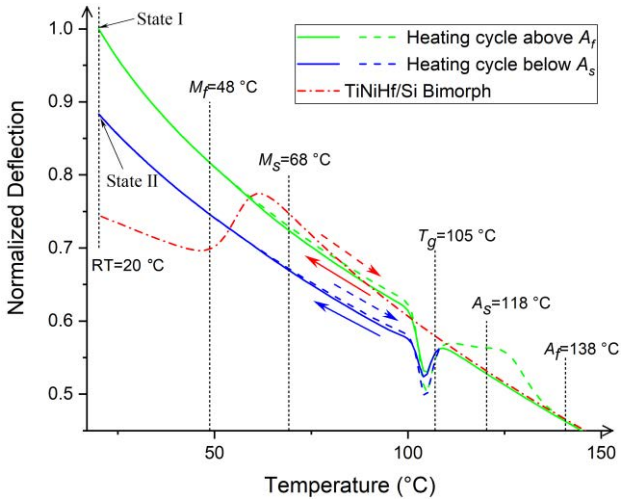

Figure 4: Simulated normalized deflection-temperature characteristics of a cantilever beam actuator consisting of a PMMA/TiNiHf/Si trimorph layer composite with layer thicknesses of PMMA: 1000 nm, TiNiHf: 220 nm, Si: 220 nm. The heating and cooling paths for bistable switching are indicated. Deflection at *State I* is taken as reference for normalization.

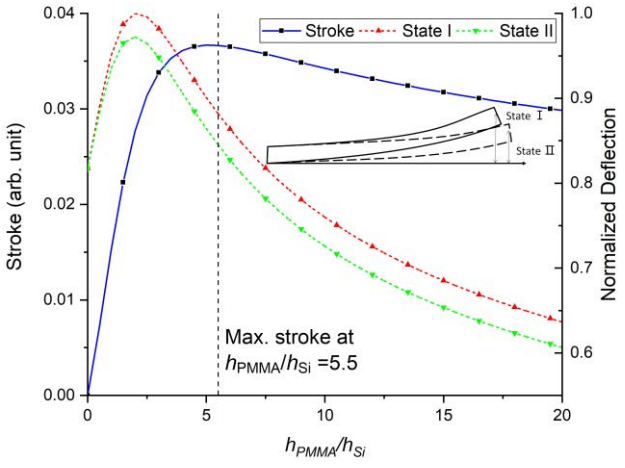

Figure 5: Simulated bistable actuation stroke versus thickness of PMMA layer given by the difference of normalized deflections in states *I* and *II*. The thicknesses of TiNiHf and Si are 220 nm.

This bistable performance depends particularly on the thickness of the PMMA layer as illustrated in **Fig. 5**. We find an optimum thickness reflecting the compromise of large enough stiffness to fix the deflection states below T_g and sufficient flexibility to adapt the deflections above T_g. Here, the difference in deflection between the two states increases dramatically when the thickness ratio between PMMA and Si grows from zero. This value reaches a peak at the ratio 5.5 and then decreases slowly with increasing thickness ratio. The large thickness ratio of 5.5 demands for a large aspect ratio of PMMA to Si structures to enable bistability.

6 Conclusion

A bistable nanoactuator consisting of a PMMA/TiNiHf/Si trimorph layer composite is presented, in which the layer of shape memory alloy TiNiHf shows a martensitic phase transformation with wide hysteresis in the temperature range of 50 - 140 °C, while the PMMA layer undergoes a glass transition at 105 °C. We demonstrate that this mechanism depends on the limitations of size effects for decreasing film thickness as well as on the thickness ratio of the PMMA to Si for a fixed TiNiHf and Si layer thicknesses of 220 nm. Our measurements reveal the existence of a critical thickness of the TiNiHf layer of 220 nm on SiO_2/Si substrates and of 440 nm on Si substrates without SiO_2 buffer layer, below which a size-dependent rapid decrease of phase transformation temperatures and a large increase of hysteresis occur. An analytical model compatible with multilayer cantilever actuators is proposed to study its deflection under thermal effect. We use this model to analyse a bistable PMMA/TiNiHf/Si three layer nanoactuator, which clearly shows two stable deflection states at RT by controlling the heating path. It is found that the actuator can have the largest deflection difference at the two states when the thickness ratio between PMMA and Si is 5.5, while the thickness of Si and TiNiHf layer are both 220 nm. Currently, the fabrication process of such trimorph nanoactuators is being explored to verify the bistable performance at the nanometer scale.

7 Literature

[1] S. Rastjoo, R. Fechner, L. Bumke, et al., *Development and co-integration of a SMA/Si bimorph nanoactuator for Si photonic circuits.* Microelectronic Engineering, 2020. **225**.

[2] P.K. Kumar and D.C. Lagoudas, *Introduction to Shape Memory Alloys*, in *Shape Memory Alloys: Modeling and Engineering Applications*. 2008, Springer US: Boston, MA. p. 1-51.

[3] R. Fechner, C. Chlub, E. Quandt, et al. *A Shape Memory Alloy 1×2 Optical Waveguide Switch*. in *2018 IEEE 18th International Conference on Nanotechnology (IEEE-NANO)*.

[4] T. Mineta and Y. Haga, *Materials and Processes in Shape Memory Alloy*, in *MEMS Materials and Processes Handbook*, Ghodssi and Lin, Editors. 2011, Springer US: Boston, MA. p. 355-402.

[5] B. Winzek, T. Sterzl, H. Rumpf, et al., *Composites of different shape memory alloys and polymers for complex actuator motions.* J. Phys. IV France, 2003. **112**: p. 1163-1168.

[6] S.M. Curtis, M. Sielenkämper, G. Arivanandhan, et al., *TiNiHf/SiO₂/Si shape memory film composites for bi-directional micro actuation.* International Journal of Smart and Nano Materials, 2022. **13**(2): p. 293-314.

[7] B. Winzek, S. Schmitz, H. Rumpf, et al., *Recent developments in shape memory thin film technology.* Materials Science and Engineering: A, 2004. **378**(1): p. 40-46.

[8] S. Timoshenko, *Analysis of Bi-Metal Thermostats.* J. Opt. Soc. Am., 1925. **11**: p. 233–255.

[9] A.M. Moulin, R.J. Stephenson, and M.E. Welland, *Micromechanical thermal sensors: Comparison of experimental results and simulations.* Journal of Vacuum Science & Technology B: Microelectronics and Nanometer Structures Processing, Measurement, and Phenomena, 1997. **15**(3): p. 590-596.

[10] T. Larsen, S. Keller, S. Schmid, et al., *Fabrication and characterization of SRN/SU-8 bimorph cantilevers for temperature sensing.* Microelectronic Engineering, 2011. **88**(8): p. 2311-2313.

[11] C.-H. Hsueh, *Modeling of elastic deformation of multilayers due to residual stresses and external bending.* Journal of Applied Physics, 2002. **91**(12): p. 9652-9656.

[12] N.-H. Zhang, *Thermoelastic stresses in multilayered beams.* Thin Solid Films, 2007. **515**(23): p. 8402-8406.

[13] S. Huang and X. Zhang, *Extension of the Stoney formula for film–substrate systems with gradient stress for MEMS applications.* Journal of Micromechanics and Microengineering, 2006. **16**(2): p. 382–389.

[14] S. Huang and X. Zhang, *Gradient residual stress induced elastic deformation of multilayer MEMS structures.* Sensors and Actuators A: Physical, 2007. **134**(1): p. 177-185.

[15] M. Batista, *Analytical treatment of equilibrium configurations of cantilever under terminal loads using Jacobi elliptical functions.* International Journal of Solids and Structures, 2014. **51**(13): p. 2308-2326.

[16] L. Chen, *An integral approach for large deflection cantilever beams.* International Journal of Non-Linear Mechanics, 2010. **45**(3): p. 301-305.

[17] J. Jiang, U. Hilleringmann, and X. Shui, *Electro-thermo-mechanical analytical modeling of multilayer cantilever microactuator.* Sensors and Actuators A: Physical, 2007. **137**(2): p. 302-307.

[18] S. Rastjoo, X. Wang, A. Ludwig, et al., *Top-down fabrication and transformation properties of vanadium dioxide nanostructures.* Journal of Applied Physics, 2019. **125**(22).

[19] F. Yang, A.C.M. Chong, D.C.C. Lam, et al., *Couple stress based strain gradient theory for elasticity.* International Journal of Solids and Structures, 2002. **39**(10): p. 2731-2743.

[20] D.C.C. Lam, F. Yang, A.C.M. Chong, et al., *Experiments and theory in strain gradient elasticity.* Journal of the Mechanics and Physics of Solids, 2003. **51**(8): p. 1477-1508.

[21] S.K. Park and X.-L. Gao, *Bernoulli–Euler beam model based on a modified couple stress theory.* Journal of Micromechanics and Microengineering, 2006. **16**(11): p. 2355–2359.

[22] E. Taati, M. Molaei Najafabadi, and H. Basirat Tabrizi, *Size-dependent generalized thermoelasticity model for Timoshenko microbeams.* Acta Mechanica, 2014. **225**(7): p. 1823–1842.

[23] H.-T. Thai, T.P. Vo, T.-K. Nguyen, et al., *A review of continuum mechanics models for size-dependent analysis of beams and plates.* Composite Structures, 2017. **177**: p. 196-219.

[24] Z.-Q. Tan and Y.-C. Chen, *Size-dependent electro-thermo-mechanical analysis of multilayer cantilever microactuators by Joule heating using the modified couple stress theory.* Composites Part B: Engineering, 2019. **161**: p. 183-189.

[25] A.S. Turabi, S. Saedi, S.M. Saghaian, et al., *Experimental Characterization of Shape Memory Alloys*, in *Shape Memory Alloy Actuators*. 2015. p. 239-277.

[26] G. Faiella and V. Antonucci, *Chapter 3 - Experimental Characterization of Shape Memory Alloys*, in *Shape Memory Alloy Engineering*, Lecce and Concilio, Editors. 2015, Butterworth-Heinemann: Boston. p. 57-77.

[27] F. Lambrecht, C. Lay, I.R. Aseguinolaza, et al., *NiMnGa/Si Shape Memory Bimorph Nanoactuation.* Shape Memory and Superelasticity, 2016. **2**(4): p. 347–359.

[28] G. Arivanandhan, Z. Li, S. Curtis, et al., *Temperature Homogenization of Co-Integrated Shape Memory—Silicon Bimorph Actuators.* Proceedings, 2020. **64**(1).

[29] G. Arivanandhan, Z. Li, S.M. Curtis, et al., *Power Optimization of TiNiHf/Si Shape Memory Microactuators.* Actuators, 2023. **12**(2).

[30] K. Ikuta and H. Shimizu. *Two dimensional mathematical model of shape memory alloy and intelligent SMA-CAD*. in *[1993] Proceedings IEEE Micro Electro Mechanical Systems*.

[31] L. Sun, T.X. Wang, H.M. Chen, et al., *A Brief Review of the Shape Memory Phenomena in Polymers and Their Typical Sensor Applications.* Polymers, 2019. **11**(6).

[32] X. Xin, L. Liu, Y. Liu, et al., *Mechanical Models, Structures, and Applications of Shape-Memory Polymers and Their Composites.* Acta Mechanica Solida Sinica, 2019. **32**(5): p. 535–565.

[33] Y. Liu, K. Gall, M.L. Dunn, et al., *Thermomechanics of shape memory polymers: Uniaxial experiments and constitutive modeling.* International Journal of Plasticity, 2006. **22**(2): p. 279-313.

[34] F.V. Loock and N.A. Fleck, *Deformation and failure maps for PMMA in uniaxial tension.* Polymer, 2018. **148**: p. 259-268.